A CHF CHARACTERISTIC FOR DOWNWARD FLOW IN A NARROW VERTICAL RECTANGULAR CHANNEL HEATED FROM BOTH SIDES

Y. Sudo and M. Kaminaga

Japan Atomic Energy Research Institute, Tokai-mura, Naka-gun, Ibaraki-ken 319-11, Japan

Abstract—A new correlation for the countercurrent flow limitation (CCFL) in vertical rectangular channels was applied to the prediction of critical heat flux (CHF) for downward flow in a vertical rectangular channel heated from both sides. The new correlation was based on CCFL experiments carried out with a two-phase flow system of air and water under 1 atm with a superficial air velocity range of 1–17 m/s. The CHF experiments were carried out with an inlet water subcooling range of 25–75 K and an inlet water mass flux range of 2–600 kg/m² s under about 1 atm for a 750 mm long, 50 mm wide and 2.25 mm gap flow channel and a 375 mm long, 50 mm wide and 2.80 mm gap flow channel which were heated from both sides. The comparison between the prediction based on the new correlation for the CCFL and the CHF experimental results could provide a good quantitative understanding of CHF characteristics, which is required for the thermal-hydraulic design and safety analysis of nuclear research reactors in which the downward flow is adopted for core cooling with flat-plate-type fuel. The role of the aspect ratio of the rectangular channel was evident in both the CCFL and CHF characteristics for countercurrent flow and it was strongly implied that the CHF for downward flow is at a minimum under the flooding condition in the case of large inlet water subcooling and when the inlet downward water mass flux is greater than that under the flooding condition in the case of small inlet water subcooling.

Key Words: critical heat flux, countercurrent flow limitation, downward flow, flat-plate-type fuel, flooding, research nuclear reactor, vertical rectangular channel, low mass flux
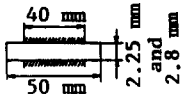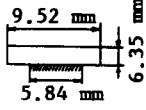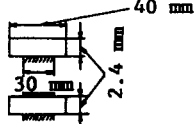
1. INTRODUCTION

The problem addressed in this study is the prediction of critical heat flux (CHF) for downward (or countercurrent) flow in a vertical rectangular channel heated from both sides, simulating a subchannel in the fuel elements of a nuclear research reactor in which downward coolant flow is adopted for core cooling with flat-plate-type fuel. The configuration of such a subchannel which is composed of the two fuel plates is rectangular and is, for example, in the case of the JRR-3, 770 mm long, 66.6 mm wide and 2.28 mm in gap (Sudo *et al.* 1985a). The core thermal-hydraulic design is such that nucleate boiling is not allowed anywhere in the core under normal operation and, on the other hand, in the safety design some abnormal operational transients and accidents have been assumed, which have a history of core flow decreasing from steady-state downward flow to zero flow and after that, establishing an upward flow as a cooling mode of natural convection to remove the decay heat after the reactor scram (Hirano & Sudo 1986). The quantitative understanding of CHF is, accordingly, essential not only for upward (or cocurrent) flow but also for downward flow, including the zero flow under the flooding condition, in order to assure the intactness of fuel under normal operation, abnormal operational transients and accidents.

A recent review by Katto (1985) gives a wide and systematic overview on CHF for both cocurrent and countercurrent flows, pointing out that the experimental data and analyses are not sufficient to fully understand the CHF for countercurrent flow. Table 1 lists the test conditions of the available existing experiments with downward flow in a rectangular channel (Yücel & Kakac 1978; Mishima 1984; Sudo *et al.* 1985b). The major parameters listed in the table are pressure, water mass flux, inlet water temperature, type of heating, configuration of the test section and ratio of the heated length to the equivalent hydraulic diameter of the flow channel.

Yücel & Kakac (1978) reported that the CHF for downward flow is a little lower than that for upward cocurrent flow for a water mass flux range of 1250–6250 kg/m² s.

Table 1. Test conditions of the available existing tests for vertical rectangular channels

Author(s)	Pressure (kg/cm² abs)	Mass flux (kg/m² s)	Inlet water temperature (K)	Type of heating	Configuration of the test section	$\dfrac{L}{D_e}$
Sudo et al. (1985b)	1.0–1.2	0–600	292–353	Heated from both sides		170, 71
Yücel & Kakac (1978)	1.0	1250–6250	331–370	Heated from one side		42
Mishima (1984)	1.0	0–600	302–360	Heated from one side Heated from both sides		77

Mishima (1984) proposed the following CHF correlation for downward flow, assuming that all downward water in the countercurrent flow would be evaporated at the lower end of the heated length under CHF conditions:

$$q_{CHF}^{*} = \left(\frac{A}{A_H}\right)\left(\frac{c_p \Delta T_{SUB}}{h_{LG}}\right) G^{*} + C^{2}\left(\frac{A}{A_H}\right) \cdot \frac{\sqrt{\dfrac{a}{\lambda}}}{\left[1 + m\left(\dfrac{\rho_G}{\rho_L}\right)^{1/4}\right]^{2}} \qquad [1]$$

and

$$\lambda = \left[\frac{\sigma}{g(\rho_L - \rho_G)}\right]^{1/2}, \qquad [2]$$

where q_{CHF}^{*} is the dimensionless CHF, A is the cross-sectional area, A_H is the heated area, c_p is the specific heat of water at constant pressure, ΔT_{SUB} is the inlet water subcooling, h_{LG} is the latent heat of evaporation, G^{*} is the dimensionless downward water mass flux, C is a constant, a is the width of the flow channel, λ is the characteristic wavelength, m is a constant, ρ_G is the vapor density, ρ_L is the water density, σ is the surface tension and g is the gravitational acceleration. The first term on the r.h.s. of [1] is the contribution of the enthalpy increase to the saturation condition of water and the second term is the heat flux in the CHF condition under flooding in the saturation condition. Equation [1] gives a clear indication that the CHF has a minimum for the condition $G^{*} = 0$ and increases with an increase in G^{*}.

Sudo et al. (1985b) carried out CHF experiments for both upward and downward flows, identifying the magnitude of error of the proposed CHF correlations for use in the core thermal-hydraulic design, and established a CHF scheme for both upward and downward flows which identifies the thresholds where the CHF for downward flow is lower than that for upward cocurrent flow.

The experimental data of both Mishima and Sudo et al. imply a close relationship between the CHF for downward flow and that in the flooding condition, i.e. under the countercurrent flow limitation (CCFL), especially for the low mass flux condition, but the relationship between the two has not been fully clarified.

This study, therefore, aims to clarify the CHF characteristics for downward flow in a vertical rectangular channel by applying the CCFL correlation for a rectangular channel to the prediction of CHF, based on the assumption that the CHF for downward flow is intimately related to the CCFL. From this point of view, CCFL experiments were first carried out for vertical rectangular channels, in order to obtain the CCFL correlation for the various values of the aspect ratio—a major parameter. The derived CCFL correlation was then applied to the prediction of CHF and the prediction was compared with the experimental results, clarifying the characteristics of CHF for downward flow in the vertical rectangular channels.

2. CCFL CORRELATION FOR VERTICAL RECTANGULAR CHANNELS

2.1. CCFL experiment

Figure 1 shows a schematic diagram of the CCFL test apparatus. The CCFL test apparatus consists of a test section, whose cross section is rectangular, an upper plenum and a lower plenum. Water supplied via the upper plenum flows down through the test section against the upward flow of air which is supplied via the lower plenum. The air is expelled to the atmosphere after flowing upward through the test section. Water is continuously supplied into the upper plenum and excess water is discharged through an overflow tube to maintain a constant water level in the upper plenum during a run.

The volumetric flow rate of water flowing down through the test section is obtained from the rate of increase in the velocity of the water level in the lower plenum and, on the other hand, the volumetric flow rate of the air is measured by rotor flowmeters.

Table 2 lists the dimensions of the test sections used in the experiment along with other major parameters. Rectangular channels were varied by changes in the size of the rectangular cross section and the length of the test section. The experiment was performed at room temperature, ~ 290 K, and 1 atm.
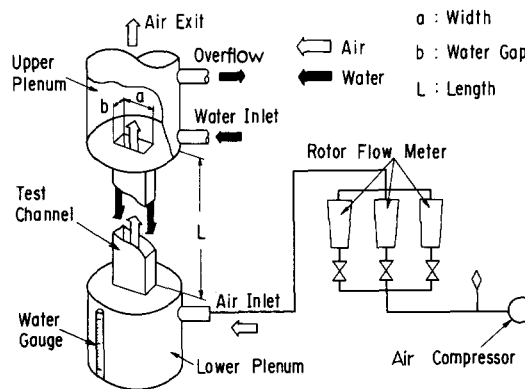

Figure 1. Schematic diagram of the CCFL test apparatus.

2.2. CCFL experimental results

In order to obtain the relationship under the CCFL condition, the following dimensionless velocities of the upward air and downward water, j_G^* and j_L^*, are used, which were originally proposed by Wallis (1969):

$$j_G^* = \left[\frac{\rho_G}{g \cdot b (\rho_L - \rho_G)} \right]^{1/2} j_G \quad \text{for air} \tag{3}$$

and

$$j_L^* = \left[\frac{\rho_L}{g \cdot b (\rho_L - \rho_G)} \right]^{1/2} j_L \quad \text{for water,} \tag{4}$$

Table 2. Experimental conditions and test channel configurations

Channel length L (mm)	72, 362, 782
Cross-section dimensions, width a × gap b (mm)	66 × 2.3, 66 × 5.3, 66 × 8.3, 66 × 12.3, 33 × 2.3, 33 × 5.3, 33 × 8.3, 33 × 12.3
Fluids used in this experiment	Water and air
Temperature (K)	288–300
Pressure (atm)	~ 1
Superficial air velocity (m/s)	1–17
Water level in the upper plenum (mm)	550

where b is the water gap of the flow channel, j_G is the superficial velocity of the gas and j_L is the superficial velocity of the water. The water gap b is adopted here as the representative length, instead of the tube diameter D which was used by Wallis.

Figure 2(a) shows the experimental data for the rectangular channel on $j_G^{*1/2}$ vs $j_L^{*1/2}$ with the water gap b and the length of test section L as parameters with a constant width of the rectangular cross section, $a = 66$ mm. The solid lines in the figure show the general trends of $j_G^{*1/2}$ vs $j_L^{*1/2}$ for each combination of a, b and L, giving the values for C and m which are defined by the following Wallis-type correlation (Wallis 1969):
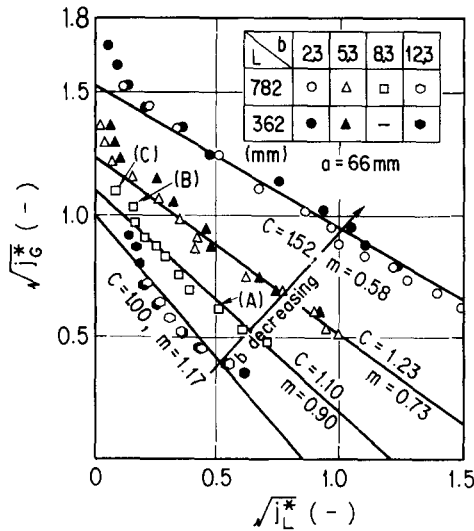
$$j_G^{*1/2} + m\, j_L^{*1/2} = C. \tag{5}$$
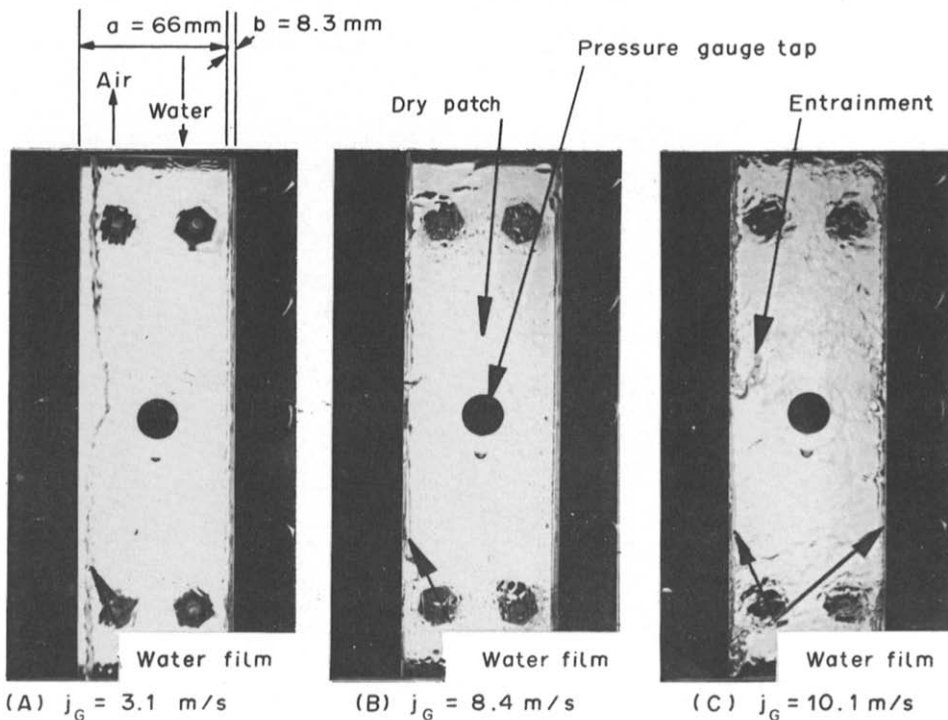

Figure 2(a)

Figure 2(b)

Figures 2(a,b). Experimental results of $j_G^{*1/2}$ vs $j_L^{*1/2}$ and flow observations in the CCFL tests.

Figure 2(a) shows the following clear trends:

(i) $j_G^{*1/2}$ increases with a decrease in $j_L^{*1/2}$ for any combination of a, b and L.
(ii) Smaller values of b give larger $j_G^{*1/2}$, for the same $j_L^{*1/2}$, a and L.
(iii) No distinct effect of L is observed on the relationship of $j_G^{*1/2}$ vs $j_L^{*1/2}$.
(iv) Smaller values of b give larger C and smaller m values, for the same a and L.

Figure 2(b) shows the variation of the flow pattern in the rectangular channel. The photographs A–C correspond to the conditions of $j_G^{*1/2}$ vs $j_L^{*1/2}$ with the same symbols as shown in figure 2(a), and the superficial air velocity was increased from photograph A to photograph C. In photograph A, a comparatively thick water film is flowing downward along the narrower side walls. On the other hand, the wider side walls are covered with a thin water film. As the superficial air velocity is increased, the wider side walls become unwetted, as shown in photograph B. With a further increase in the air velocity, the interaction between the downward water film and the upward air flow becomes significant, as shown in photograph C. Disturbance waves appear on the water film. Water droplets begin to be entrained and the wider side walls do, therefore, become wetted again.

2.3. Introduction of the new CCFL correlation

Figures 3(a,b) show the effects of the aspect ratio b/a of the rectangular cross section and the Bond number Bo on the constants C and m. The Bo was found in this study, through a dimensional analysis, to be another dominant dimensionless parameter and is defined as follows:

$$Bo = \frac{a \cdot b(\rho_L - \rho_G)g}{\sigma}. \quad [6]$$

The constant C defined in [5] is well-correlated with the aspect ratio b/a by the following expression:

$$C = 0.66 \left(\frac{b}{a}\right)^{-0.25}, \quad [7]$$

which is a function of the aspect ratio alone. This expression shows the experimental tendency, already described, that smaller values of b give larger C values, for the same a and L and, at the same time, that larger values of a give larger C values, for the same b and L.

On the other hand, the constant m also defined in [5], is well-correlated with solely the Bo by the following expression:

$$m = 0.5 + 0.0015 \, Bo^{1.3}. \quad [8]$$

This expression shows that the constant m actually increases with an increase in either a or b, reflecting the tendency already described that smaller b gives smaller m for the same a and L.

Figure 4 shows a rearrangement of the experimental data of $j_G^{*1/2}$ vs $j_L^{*1/2}$ for the combinations of a, b and L, introducing the following new dimensionless parameters for the abscissa and the ordinate, based on the expressions for C and m obtained in [7] and [8]:

$$X = \frac{m}{C} j_L^{*1/2} = 1.52 \left(\frac{b}{a}\right)^{0.25} (0.5 + 0.0015 \, Bo^{1.3}) j_L^{*1/2} \quad [9]$$

and

$$Y = \frac{1}{C} j_G^{*1/2} = 1.52 \left(\frac{b}{a}\right)^{0.25} j_G^{*1/2}. \quad [10]$$
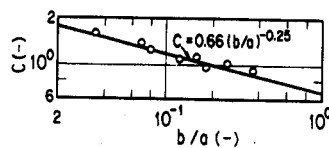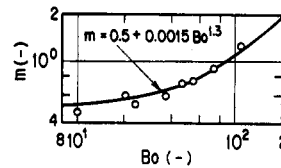

Figure 3(a)

Figure 3(b)

Figures 3(a,b). Effects of the aspect ratio b/a and Bo on m and C in the CCFL tests.
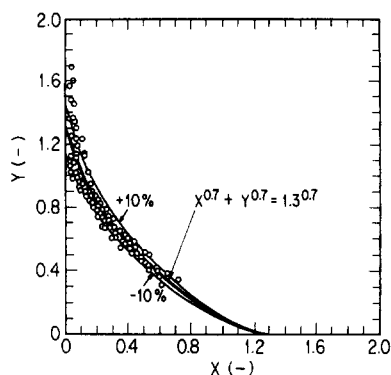
Figure 4. CCFL correlation of X vs Y in this study.

All the data obtained in the experiment were well-correlated with the aspect ratio b/a and the Bo by the following correlation:

$$X^{0.7} + Y^{0.7} = 1.3^{0.7}. \tag{11}$$

The magnitude of error of [11] to the experimental data is estimated to be within about $\pm 10\%$, as shown in figure 4.

3. CHF EXPERIMENTS FOR VERTICAL RECTANGULAR CHANNELS

3.1. CHF experiments

Figure 5(a) shows a schematic diagram of the CHF test loop. The CHF test loop is composed of a coolant storage tank, a recirculation line and a test section with a rectangular channel in it. Water is used as a coolant in this study. The coolant storage tank has a cooling line in it to keep the inlet water temperature constant during a test. The tank is open to the atmosphere. The recirculation line has a pump, a bypass line, a rotor flowmeter, an electromagnetic flowmeter, stop valves and regulation valves.

The test section has a lower plenum and an upper plenum at the lower and upper ends, respectively. Two kinds of test section were used: one is 750 mm long, 50 mm wide and 2.25 mm in water gap; and the other is 375 mm long, 50 mm wide and 2.80 mm in water gap. The heating plates are made of Inconel 600, 1 mm thick and 40 mm wide. A detailed cross section of the test section is shown in figure 5(b). The heating plates are mounted on the thermal insulator in the frame of the test section. The inside of the flow channel can be observed through the lucite window. Sheathed thermocouples of 0.5 mm o.d. are welded on to the back surface of the heating plates along the heated length to detect the CHF condition: with 20 thermocouples attached on one heating plate and 10 thermocouples on the other for the test section with the longer heated length
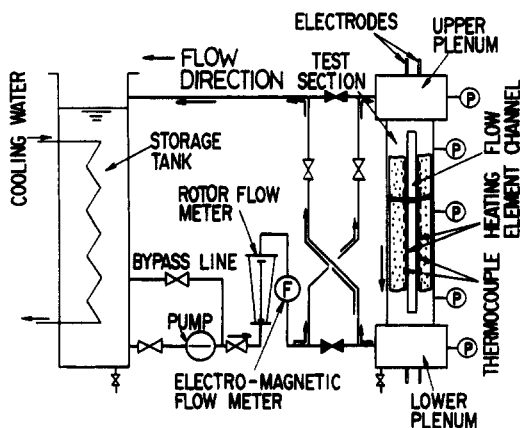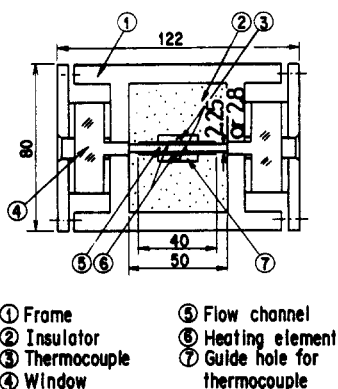

Figure 5(a)

Figure 5(b)

Figures 5(a,b). Schematic diagram of the CHF test apparatus and test section.

Table 3. Test conditions of the CHF experiments for downward flow in the
vertical rectangular channel in this study

Flow channel	750 mm long, 50 mm wide, 2.25 mm gap
	375 mm long, 50 mm wide, 2.8 mm gap
Heating plates	750 mm long, 40 mm wide, 1 mm thick
	375 mm long, 40 mm wide, 1 mm thick
Type of heating	Heated from both sides
Coolant	Water
Pressure (atm)	~ 1
Inlet subcooling (K)	25, 75
Water mass flux (kg/m² s)	2–600

($L = 750$ mm); and with 10 and 5 thermocouples on each heating plate for the test section with the shorter heated length ($L = 375$ mm), respectively.

Instrumentation items are the water flow rate, the heat input into the channel, the coolant temperatures at the inlet and outlet of the channel, the coolant pressures in the channel and the surface temperatures of the heating plates. The heating plates are heated by direct current and the heat input into the channel is determined by measurements of current and voltage for each of the heating plates. The inlet and outlet coolant temperatures are measured with 1.6 mm o.d. thermocouples installed in the upper and lower plena.

The major parameters of the experiment are the heat input, the downward flow rate of the water, the inlet coolant temperature and the heated length of the flow channel. The ranges of these parameters investigated in the experiment are listed in table 3. The experiment covers a velocity range of about 0.002–0.6 m/s.

3.2. CHF experimental results

3.2.1. Flow observation. Flow observation should be helpful in understanding the mechanism of occurrence of the CHF for downward flow.

In the case of a downward flow whose temperature was lower than the saturation temperature at the inlet of the channel, an increase in the heat input changed the flow in the channel from a single-phase water flow to a subcooled boiling two-phase flow, in which vapor bubbles generated on the surfaces of the heating plates went downward accompanied by the downward flow of water. A further increase in the heat input resulted in the occurrence of alternate cocurrent downward flow and countercurrent flow. In the cocurrent downward flow, water and vapor bubbles generated in the channel went down through the channel. In the countercurrent flow, the vapor bubbles went upward and the water went down, but at the onset of the countercurrent flow, the vapor bubbles disappeared or stopped going upward before the vapor bubbles reached the upper end of the heated length. With a further increase in the heat input, the occurrence of alternate cocurrent downward flow and countercurrent flow continued with the vapor bubbles reaching the upper end of the heated length in the countercurrent flow, and at last the CHF condition occurred.

Therefore, as has been reported by Mishima (1984), it is reasonable to consider that the occurrence of the CHF condition in the downward flow is intimately related to the occurrence of alternate cocurrent downward flow and countercurrent flow with the vapor bubbles reaching the upper end of the heated length in the countercurrent flow. The CHF condition is, then, considered to occur under the countercurrent flow condition in the downward water flow. It should be noted here that the water supplied into the flow channel at the inlet of the flow channel is still going down through the lower end of the flow channel, even in the CHF condition where not all the water has evaporated in the flow channel. This is not consistent, in a strict sense, with the assumption adopted by Mishima (1984) and Sudo *et al.* (1985b).

3.2.2. Experimental correlation of q_{CHF}^* vs G^*. In this study, two fundamental dimensionless parameters representing the CHF and the inlet water mass flux under the CHF condition are introduced, which are defined as

$$q_{CHF}^* = \frac{q_{CHF}}{h_{LG}\sqrt{\lambda\rho_G(\rho_L - \rho_G)g}}$$
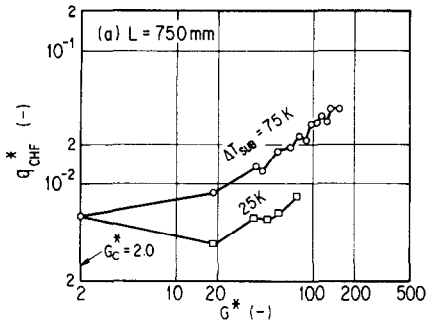
[12]

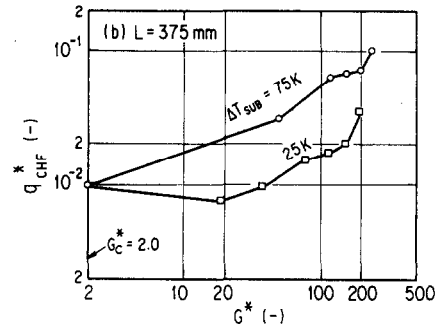Figure 6(a)   Figure 6(b)

Figures 6(a,b). Experimental results of q_{CHF}^* vs G^* for downward flow in a vertical rectangular channel obtained in this study.

and

$$G^* = \frac{\rho_L j_{Li}}{\sqrt{\lambda \rho_G (\rho_L - \rho_G)g}},$$ [13]

where q_{CHF} is the critical heat flux and j_{Li} is the inlet water superficial velocity. These parameters have already been proposed by Mishima (1984) to correlate with each other for the prediction of CHF. They are adopted here also because they are convenient to correlate the CHF data obtained at different pressures.

Figures 6(a,b) show the experimental data of q_{CHF}^* vs G^* for $L = 750$ and 375 mm, respectively. The inlet water subcooling ΔT_{SUB} is adopted as a parameter. It should be noted here that G^* is defined in [13] for the inlet water mass flux. The G^* under the flooding condition represented by G_c^* is then obtained by the simultaneous equations of [11] and mass conservation, given by $\rho_L j_{Li} = \rho_G j_{Gi}$, because no water goes down through the lower end of the flow channel. The calculated result for G_c^* is shown below:

$$G_c^* = \frac{X_0^2}{\left\{ \frac{0.5 + 0.0015\left[\dfrac{a \cdot b(\rho_L - \rho_G)g}{\sigma}\right]^{1.3}}{0.66\left(\dfrac{b}{a}\right)^{-0.25}} \right\}^2 \cdot \left[\dfrac{\lambda \rho_G}{b(\rho_L - \rho_G)}\right]^{1/2}},$$ [14]

where

$$X_0 = \frac{1.3}{\left[1 + \dfrac{\left(\dfrac{\rho_L}{\rho_G}\right)^{0.175}}{\left\{0.5 + 0.0015\left[\dfrac{a \cdot b(\rho_L - \rho_G)g}{\sigma}\right]^{1.3}\right\}^{0.7}}\right]^{1/0.7}}.$$ [15]

For the conditions of the present experiment, the value of G_c^* is 2.0 for both test sections with $L = 750$ and 375 mm. Values > 2.0 are shown on the abscissas in figures 6(a,b). The figures show the following clear CHF tendencies:

(i) A higher inlet water subcooling ΔT_{SUB} gives a higher CHF.
(ii) A shorter heated length L gives a higher CHF.
(iii) For $G^* > 20$, a larger G^* gives a higher CHF.
(iv) In the case of $\Delta T_{SUB} = 25$ K, the CHF becomes a minimum for $G^* = 20$; while in case of $\Delta T_{SUB} = 75$ K, the CHF becomes a minimum for $G^* = 2.0$ (under the flooding condition).
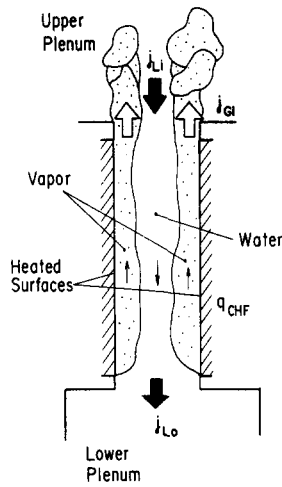
Figure 7. Flow model for the CHF condition in downward flow.

4. COMPARISON BETWEEN CHF PREDICTION BASED ON THE NEW CCFL CORRELATION AND THE EXPERIMENTAL RESULTS

4.1. Application of the new CCFL correlation to CHF prediction

We consider the following model with the countercurrent flow pattern shown in figure 7:

(i) Upward steam generated in the test section and the downward water are completely separated under the countercurrent flow condition.

(ii) Water is introduced in the test section with constant inlet water subcooling ΔT_{SUB}. The CHF condition is assumed to occur after the water becomes saturated in the test section.

(iii) The CHF condition is assumed to be given by the CCFL correlation, which gives the maximum upward steam flow rate under the given downward water flow rate. The new CCFL correlation [11] is used as the CCFL correlation.

(iv) Under the CHF conditions the water supplied into the test section is assumed to be still going down through the lower end of the test section, i.e. it is not necessary for all the water in the test section to have evaporated, except for under the flooding conditions.

The energy balance for the CHF condition is given by

$$q_{CHF} A_H = h_{LG} A \rho_G j_{Gi} + c_p \Delta T_{SUB} A \rho_L j_{Li}. \qquad [16]$$

The new CCFL correlation, introduced in section 2.3, is rewritten as

$$\left[1.52 \left(\frac{b}{a} \right)^{0.25} j_{Gi}^{0.5} \left(\frac{\rho_G}{g \cdot b(\rho_L - \rho_G)} \right)^{0.25} \right]^{0.7}$$

$$= 1.3^{0.7} - \left[1.52 \left(\frac{b}{a} \right)^{0.25} (0.5 + 0.0015 \, Bo^{1.3}) j_{Li}^{0.5} \left(\frac{1}{g \cdot b} \right)^{0.25} \right]^{0.7}. \qquad [17]$$

From [16] and [17], the following correlation is obtained for q_{CHF}^* vs G^*, which were defined in [12] and [13], respectively:

$$q_{CHF}^* = \left(\frac{A}{A_H} \right) \left[\left(\frac{c_p \Delta T_{SUB}}{h_{LG}} \right) G^* + \left(\frac{1}{1.52} \right)^2 \left(\frac{a}{\lambda} \right)^{0.5} F^{2.875} \right], \qquad [18]$$

where

$$F = 1.3^{0.7} - \left[1.52 \left(\frac{\lambda}{a} \frac{\rho_G}{\rho_L} \right)^{0.25} (0.5 + 0.0015 \, Bo^{1.3}) G^{*0.5} \right]^{0.7}. \qquad [19]$$
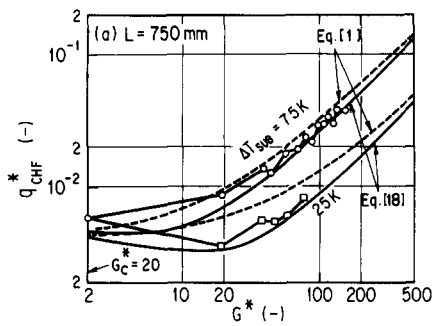
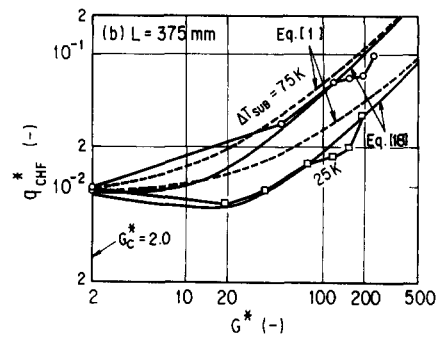Figure 8(a)   Figure 8(b)

Figures 8(a,b). Comparison of CHF between the prediction based on the new CCFL correlation and the experimental results in this study.

4.2. Comparison between the prediction and experimental results

Figures 8(a,b) show the comparison between the prediction and the experimental results on q^*_{CHF} vs G^*. The solid lines show the predictions given by [18] and the dotted lines show the predictions given by [1], with $C^2 = 0.7$, m = 1 and using a as the representative length in [1], after Sudo et al. (1985b); Mishima (1984) proposed $C^2 = 0.533$ for the test section heated from one side and $C^2 = 0.4$ for the test section heated from both sides, using a as the representative length in [1]. This is because the former showed a much better agreement with the experimental results than the latter, as reported by Sudo et al. (1985b). The q^*_{CHF} prediction given by [18] is, in general, smaller than that given by [1], especially in the range of G^* from 5 to 200. It should be emphasized that in figures 8(a,b) the solid lines show far better agreement with the experimental results for different test section lengths, especially in the case of small subcooling. The key result is that the solid lines show the clear tendency, observed in the experiment, that q^*_{CHF} is a minimum, not in the flooding conditions, but for the conditions where $G^* \sim 20$ in the case of smaller inlet water subcooling, $\Delta T_{SUB} = 25$ K. This agreement is observed for both the cases $L = 750$ and 375 mm. The experimental tendency described above is not predicted by [1].

Figure 9 shows the comparison between the prediction by [18] and the experimental results of Mishima (1984) for the case of a test section heated from one side. The comparison was made for the test section length $L = 350$ mm and inlet water subcooling $\Delta T_{SUB} = 70$ and 15 K. Also, in Mishima's experiment there appears the same tendency as in figures 8(a,b), that q^*_{CHF} is a minimum for $G^* \sim 20$ in the case of smaller inlet water subcooling $\Delta T_{SUB} = 15$ K. The predictions of q^*_{CHF} given by [18] also show much better agreement with the experimental results than that given by [1] in the case of a test section heated from one side. In figure 9, $G^* > 1.8$ is shown on the abscissa because G^*_c under the flooding condition is 1.8 for the test section used by Mishima (1984).
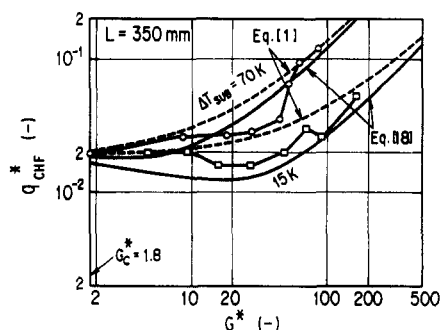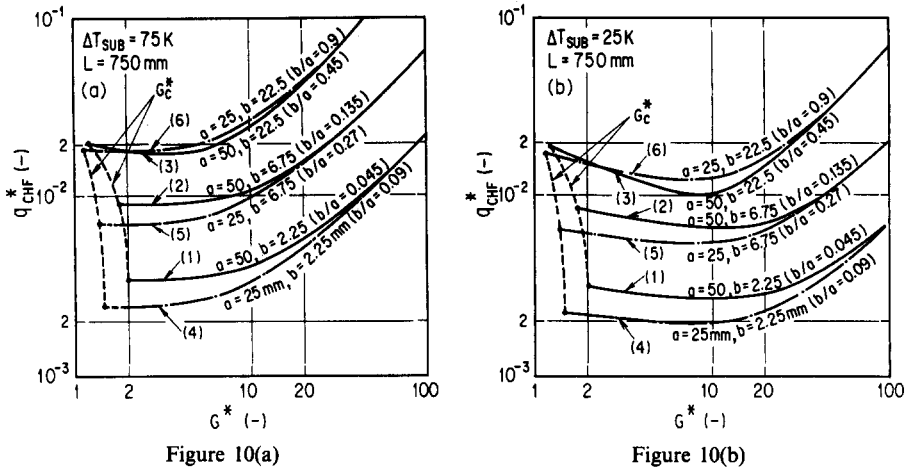

Figure 9. Comparison of CHF between the prediction based on the new CCFL correlation and the experimental results of Mishima (1984).

Figure 10(a)

Figure 10(b)

Figures 10(a,b). Effects of the aspect ratio b/a for the inlet water subcooling $\Delta T_{SUB} = 75$ and 25 K with the heated length $L = 750$ mm, derived by [18].

4.3. Effects of the aspect ratio b/a on q^*_{CHF} vs G^*

Figures 10(a,b) show the effects of the aspect ratio b/a of rectangular channels on q^*_{CHF}, based on the prediction given by [18]. The effects are shown for the two cases $\Delta T_{SUB} = 75$ and 25 K, for a flow channel of length $L = 750$ mm. The following tendencies can be observed with respect to the effects of the aspect ratio:

(i) For the same flow channel width a, the q^*_{CHF} increases as the water gap b increases. The q^*_{CHF} does, therefore, increase with an increase in the aspect ratio.

(ii) The q^*_{CHF} increases as the flow channel width a increases for $b = 2.25$ and 6.75 mm, but the q^*_{CHF} decreases as the flow channel width a increases for $b = 22.5$ mm.

(iii) The magnitude of the effect of the flow channel width a is smaller than that of the water gap b.

From the results described above, it is concluded that the q^*_{CHF} given by [18] increases with an increase in b and b/a.

The calculated results of q^*_{CHF} vs G^*_c under the flooding conditions are also shown in figures 10(a,b). It can be easily understood that the larger aspect ratio b/a gives the smaller G^*_c, giving the larger q^*_{CHF}. This is the effect of the aspect ratio on q^*_{CHF} and G^*_c under the flooding conditions predicted by [14] and [18].

5. CONCLUSION

A new correlation was proposed for the CCFL in vertical rectangular channels and was applied to the prediction of CHF for downward flow in a vertical rectangular channel heated from both sides, which is required for the thermal-hydraulic design and safety analysis of nuclear research reactors in which downward flow is adopted for core cooling with flat-plate-type fuel.

The new CCFL correlation was obtained by experiments with a two-phase flow system of air and water under 1 atm with a superficial air velocity of 1–17 m/s, and revealed an important effect of the aspect ratio of the rectangular channel on the CCFL characteristics. The CHF prediction based on the new CCFL correlation was compared with the results of the experiments, which were carried out for both a 750 mm long, 50 mm wide and 2.25 mm gap flow channel and a 375 mm long, 50 mm wide and 2.80 mm gap flow channel which were heated from both sides under about 1 atm, with inlet water subcoolings of 25 and 75 K, respectively, and inlet downward water mass fluxes of 2–600 kg/m² s.

The results made the following points clear:

(i) The new CHF prediction for downward flow in vertical rectangular channels based on the new CCFL correlation shows a much better coincidence with the

experimental results than the prediction based on the existing flooding correlation, making clear the previously undetermined role of the aspect ratio of the rectangular channel.

(ii) It was strongly implied, both analytically and experimentally, that the CHF for downward flow is a minimum under the flooding condition in the case of large inlet water subcooling and for an inlet downward water mass flux larger than that under the flooding condition in the case of small inlet water subcooling.

REFERENCES

HIRANO, M. & SUDO, Y. 1986 Analytical study on the thermal-hydraulic behavior of the transient from forced circulation to natural circulation in JRR-3. *J. nucl. Sci. Technol.* **23**, 352–368.

KATTO, Y. 1985 Critical heat flux. In *Advances in Heat Transfer*, Vol. 17 (Edited by HARTNETT, J. P. & IRVINE, T. F. JR), pp. 2–64. Academic Press, New York.

MISHIMA, K. 1984 Boiling burnout at low flow rate and low pressure conditions. Dissertation Thesis, Kyoto Univ.

SUDO, Y., ANDO, H., IKAWA, H. & OHNISHI, N. 1985a Core thermohydraulic design for the upgraded JRR-3 with 20% LEU fuel. *J. nucl. Sci. Technol.* **22**, 551–564.

SUDO, Y., MIYATA, K., IKAWA, H., KAMINAGA, M. & OHKAWARA, M. 1985b Experimental study of differences in DNB heat flux between upflow and downflow in vertical rectangular channel. *J. nucl. Sci. Technol.* **22**, 604–618.

WALLIS, G. B. 1969 *One-dimensional Two-phase Flow*, pp. 336–339. McGraw-Hill, New York.

YÜCEL, B. & KAKAC, S. 1978 Forced flow boiling and burnout in rectangular channel. *Proc. 6th Int. Heat Transfer Conf.* **1**, 387–392.